Biofilm Derived Oxylipin Mediated Autoimmune Response in Breast Implant Subjects

Imran Khan[1], Robert E. Minto[2], Christine Kelley-Patteson[3], Bruce W. Van Natta[3], Colby R. Neumann[1], Lily J. Suh[1], Kanhaiya Singh[1], Mary Lester[4], R Jason VonDerHaar[4], Gayle M. Gordillo[1], Aladdin H. Hassanein[1], Chandan K. Sen[1], Marshall E. Kadin[5,6], Mithun Sinha[1*]

[1]*Indiana Center for Regenerative Medicine and Engineering, Department of Surgery, Division of Plastic Surgery, Indiana University School of Medicine, Indianapolis, Indiana, USA*

[2]*Department of Chemistry and Chemical Biology, Indiana University-Purdue University Indianapolis, Indianapolis, Indiana*

[3]*Meridian Plastic Surgeons, Indianapolis, Indiana*

[4]*Division of Plastic Surgery, Department of Surgery, Indiana University School of Medicine, Indianapolis, Indiana,*

[5]*Department of Dermatology, Roger Williams Medical Center, Boston University School of Medicine, Providence, Rhode Island, USA*

[6]*Warren Alpert School of Medicine, Brown University, Providence, Rhode Island*

[*] Corresponding Author: Mithun Sinha, PhD; mitsinha@iu.edu

Address: 975 W Walnut St,

                          Medical Research Library Building, Suite # 444A

                          Indiana University School of Medicine

                          Indianapolis, IN 46202.

                          Tel. 317 278 2713

                          Fax. 317 278 2708

Short Title: Biofilm mediated autoimmune response

Abstract

Over 10 million women worldwide have breast implants for breast cancer/prophylactic reconstruction or cosmetic augmentation. In recent years, a number of patients have described a constellation of symptoms that are believed to be related to their breast implants. This constellation of symptoms has been named Breast Implant Illness (BII). The symptoms described include chronic fatigue, joint pain, muscle pain and a host of other manifestations often associated with autoimmune illnesses. In this work, we report that bacterial biofilm is associated with BII. We postulate that the pathogenesis of BII is mediated *via* a host-pathogen interaction whereby the biofilm bacteria *Staphylococcus epidermidis* interacts with breast lipids to form the oxylipin 10-HOME. The oxylipin 10-HOME was found to activate CD4$^+$ T cells to Th1 subtype. An increased abundance of CD4$^+$Th1 was observed in the breast tissue of BII subjects. The identification of a mechanism of immune activation associated with BII via a biofilm enabled pathway provides insight into the pathogenesis for implant-associated autoimmune symptoms.

Introduction

Breast implants were first introduced in 1962. Nearly 60 years later, their safety has continued to be controversial in the medical field, including a period of FDA-mandated restrictions on the use of silicone gel breast implants in the U.S. in the 1990s[1, 2]. Nearly 300,000 women have breast implant surgeries every year in the United States, for reasons including cosmetic augmentation, post-mastectomy breast reconstruction (breast cancer and prophylactic mastectomy), revision of prior augmentation/ reconstruction, and gender affirmation[3]. A subset of patients with breast implants have a myriad of nonspecific systemic symptoms[4, 5]. The symptoms described include fever, myalgias, chronic fatigue, arthralgias and a host of other manifestations often associated with autoimmune illnesses[6-12]. This constellation of symptoms related to implants has been named Breast Implant Illness (BII). The number of patients who opt for breast implant explantation due to complications including breast implant illness is over 30,000 annually[3]. Thus, BII is a growing concern to both patients and surgeons alike with more than 10 million women worldwide currently having breast implants[6]. Despite the increased concern regarding BII, existing scientific literature doesn't show a definite link between breast implants and autoimmune or connective tissue diseases. Some epidemiological studies have reported that women with silicone gel-filled implants were 8 times more likely to be diagnosed with Sjögren syndrome, an autoimmune disorder characterized by dry eyes and a dry mouth. Also, such subjects are 7 times more likely to be diagnosed with scleroderma, a group of autoimmune diseases that cause the skin and connective tissues to become hard and tighten, and nearly 6 times more likely to be diagnosed with rheumatoid arthritis[8]. Other studies have reported an association of autoimmune symptoms with breast implants[7, 9-12]. Symptoms have been documented to begin after placement of the implant and are often relieved by their explantation [13, 14]. This led patients and physicians to suspect that the breast implants are the likely cause [13, 14]. However, FDA mandated studies have found silicone gel breast implants to be safe[15]. Of note to this apparent contradiction is the fact that

71 these symptoms have been reported in subjects with other implants such as orthopedic

72 arthroplasty which is typically comprised of titanium[16-20]. This indicates that the underlying cause

73 of these conditions may be associated with factors other than the implant material. Therefore, it

74 is important to decipher the underlying molecular mechanism associated with BII for a better

75 understanding in the future of all implant-related illnesses with autoimmune manifestations.

76 This is the first in depth study to investigate the possible role of bacterial biofilm as a factor in the

77 pathogenesis of BII through a patient-based study with a mechanistic pathway. We have identified

78 a biofilm-derived oxylipin in increased abundance in BII subjects. The oxylipin led to activation of

79 CD4^{+} Th1 cells in an *in vitro* and *in vivo* mouse model suggesting a role in the establishment of

80 an autoimmune response often observed to be associated with BII.

81

82 ## Results

83 **Bacterial Biofilm in Implant-Associated with BII**

84 The study included 68 patients. Forty-six patients with BII were analyzed. Subjects were

85 diagnosed with BII using clinical parameters outlined in previous studies [6-12] **(Fig. 1A)** . As a part

86 of the diagnosis, the patients were required to complete a questionnaire **(Supplementary Table**

87 **1)**. The questionnaire screened for the commonly reported symptoms associated with BII [6-12].

88 Implant, associated capsules and breast tissue were collected from these subjects **(Fig. 1B-C)**

89 as described in methods. The mean age of BII patients was 44.0 years with mean duration of

90 implant insertion of 11.51 years. Two groups were considered as controls. Control group I (non-

91 BII, n=14) was comprised of patients with breast implants who didn't exhibit BII symptoms but

92 went through explantation of the breast implant. The mean age of non-BII patients was 46.5 years.

93 Control group II (normal tissue, n=8) was comprised of patients without an implant, whose breast

94 tissue was removed as a clinically indicated surgical procedures e.g., (breast reduction surgery,

95   mammoplasty, contralateral procedures for reconstruction symmetry and mastopexy). The mean

96   age of normal subjects was 26.8 years. The demographics of the subjects have been provided in

97   **Supplementary Table 2**.

98   Bacterial biofilm was observed in implant-associated capsules through scanning electron

99   microscopy **(Fig. 1D, Supplementary Fig. S1A)**. Though biofilm was detected in the capsules of

100   implants from both BII and non-BII patients, the abundance of biofilm was significantly more in

101   the capsules of BII subjects as observed through wheat germ agglutin (WGA) assay **(Fig 1E-F)**.

102   The microbiological culture analyses of the tissues resulted in no growth of bacterial colonies

103   (data not shown). It has been reported that bacterial biofilms are difficult to detect through colony

104   forming assays due to their subdued metabolism [21, 22]. Hence, in cases of bacterial biofilm, next

105   generation sequencing (NGS) using variable region of bacterial 16S rRNA gene are employed to

106   type bacteria and determine their abundance[23]. Diverse types of biofilm forming bacteria were

107   observed associated with BII, non-BII and normal tissues **(Fig. 1G-I)** through next generation

108   sequencing (NGS) of the 16S rRNA variable region. Most of the species identified were

109   opportunistic bacteria associated with normal skin flora capable of forming biofilms. **(Fig. 1G-I)**.

110   Comparative analyses with the normal, non-BII and BII groups revealed an increased abundance

111   of *Staphylococcus epidermidis* in BII **(Fig. 1J)**. The other bacteria found in increased abundance

112   in breast tissue was *Cutibacterium acnes*. Bivariate analysis using cross-tabulation was

113   performed between presence of biofilm and the study groups. Using the Fisher's exact test,

114   *Staphylococcus epidermidis* colonization was observed to be significantly higher (p<0.001) in the

115   BII group (63.04%) compared to non-BII group (14.3%) and the normal group. Using exact logistic

116   regression, the BII group was 9.8 times significantly more likely to have *S. epidermidis*

117   colonization compared to the non-BII group (p=0.003). Similarly, when comparing with normal

118   groups, the BII group was 17.4 times significantly more likely to have *S. epidermidis* (p=0.0021).

119   *C. acnes* was not found to be associated (Fisher's exact p-value=0.116) with the groups defined

120   in the study. However, though not significant, the BII group (80.4%) tended to show 4 times higher

121   odds of colonization with *C.acnes* (Odds ratio from exact logistic regression=3.98 [95% CI: 0.32,

122   26.10, p=0.1684]) compared to the normal (50.0%) group **(Fig. 1J, Supplementary Fig. S1B)**.

Increased Abundance of Biofilm Derived 10-HOME in BII Subjects

124   The oxylipin (10)-hydroxy-(8*E*)-octadecenoic acid (10-HOME) is formed by the bacterial oxidation

125   of oleic acid **(Fig. 2A)**. The oxylipin 10-HOME has been reported to inhibit flagellum-driven

126   swimming and swarming motilities and stimulate the formation of bacterial biofilms *in vitro*[24]. The

127   oxylipin 10-HOME was synthesized in the laboratory (commercially not available) in natural

128   isotopic abundance (light) isotope and deuterated (heavy) isotope forms. The former was used

129   for biological experiments, whereas the later was used as a liquid chromatography-mass

130   spectrometry (LC-MS) standard. The synthesized 10-HOME was validated through thin layer

131   chromatography and NMR spectroscopy **(Supplementary Fig. S2A-B)**.

132   Elevated levels of 10-HOME in implant-associated samples of BII compared to non-BII samples

133   were observed through mass spectrometry (**Fig. 2B-D**). Positive correlation was observed

134   between bacterial abundance and concentration of 10-HOME in BII subjects **(Fig. 2E)**. Similar

135   correlation was observed in BII subjects with *Staphylococcus epidermidis* **(Fig. 2F)**. To determine

136   if *S. epidermidis* was capable of synthesizing 10-HOME, it was cultured *in vitro* with oleic acid as

137   a source of carbon. Formation of 10-HOME was detected using gas chromatography-mass

138   spectrometry **(Fig. 2G)**. Oxylipins have been reported to cause CD4$^+$ T cell activation[25]. Hence,

139   we explored the role of CD4$^+$ T cells in BII.

Abundance of CD4$^+$ Th1 Cells in Implant-Associated Tissue of BII Subjects

141   Breast tissue associated with the implant of BII subjects showed increased presence of CD4$^+$

142   T-BET$^+$ T cells compared to that of non-BII breast tissue **(Fig. 3A)**. T-BET transcription factor is

143   critical in Th1 subtype determination[26]. Th1 cells are associated with an auto-immune response

144   in multiple illnesses including rheumatoid arthritis[27]. The CD4^{+} Th1 cells associated with BII

145   subjects also were CD36^{+} **(Fig. 3B)**. CD36 is a fatty acyl translocase[28]; its level is upregulated

146   when uptake of fatty acid (normal or oxidized) is required. It is to be noted that BII is a systemic

147   autoimmune manifestation. Hence, the peripheral blood of BII and non-BII subjects was analyzed

148   for CD4^{+} T cells (Th1, Th2, Th9 and Th22). Increased abundance of Th1 cells was observed in

149   BII subjects (N=9) as measured through flow cytometry using CD183/CXCR3 (CD4^{+} Th1 cell

150   marker) **(Fig. 3C)**. No significant difference was observed in the abundance of other Th subtypes

151   Th2 (CD194), Th9 (CD196) and Th22 (CD196) between BII subjects and non-BII subjects

152   **(Supplementary Fig. S3A-B)**. The following human cell lines were used as positive control for

153   validation of surface antigens. Mac2A for CD183, Mac2B for CD194[29] and TLBR1 for CD196[30]

154   **(Supplementary Fig. S3C-E)**. These results, however, don't definitively establish that 10-HOME

155   led to CD4^{+}Th1 cell induction or that 10-HOME can lead to CD36 upregulation. Thus, we studied

156   the effect of 10-HOME on human primary naïve CD4^{+} T cells.

157

158   **Oxylipin 10-HOME Polarizes Naïve CD4+ T Cells to Th1 Subtype *in vitro***

159   In order to study the effect of 10-HOME on T cells, naïve CD4^{+} T cells (isolated from human

160   peripheral blood mononuclear cells) were treated with 100 µM 10-HOME for 48h. Increased CD36

161   expression was observed in the 10-HOME treated CD4^{+} T cells through immunocytochemistry

162   **(Fig. 4A)**, flow cytometry **(Fig. 4B)** and quantitative real time PCR **(Fig. 4H)** indicative of the 10-

163   HOME mediated induction of CD36. Polarization to Th1 subtype occurred in the presence of 10-

164   HOME as observed through immunocytochemistry **(Fig. 4C)**, flow cytometry **(Fig. 4D)**, and

165   quantitative real time PCR **(Fig. 4I)**. The CD4^{+} cells exhibited increased expression of T-BET (a

166   transcription factor activated during the polarization of naïve T cells to Th1 subtype[26])**(Fig. 4C,**

167   **4H, Supplementary Fig. 4A**), CD183/ CXCR3 (CD4^{+} Th1 cell marker) (**Fig. 4D**), and Th1

168   secreted pro-inflammatory cytokine IFN-γ through ELISA (**Fig. 4E**). The CD183+ Th1 cells

169   exhibited increased abundance of CD36 marker (**Supplementary Fig. 4B**). The other subtypes

170   of CD4+ T cells (Th2, Th9 and Th22) assayed didn't exhibit any statistically significant increase in

171   abundance post 10-HOME treatment on naïve CD4+ T cells. Th2 cells were assayed using

172   surface marker CD194/CCR4 (**Supplementary Fig. 4C**), transcription factor GATA3

173   (**Supplementary Fig. 4D**) and anti-inflammatory cytokines IL 4 and IL10 (**Fig. 4F-G**). Th9 and

174   Th22 cells were assayed using surface marker CD196/CCR6 (**Supplementary Fig. 4E**).

175

176   **Elevated CD4+ Th1 in Peripheral Blood of Mice Administered with 10-HOME**

177   To test if 10-HOME can induce Th1 cells *in vivo*, we administered 10-HOME into the abdominal

178   mammary fat pad of mice (**Fig. 5A**) as described in the Methods. An increased abundance of

179   CD4+ Th1 cells was found in the murine blood 14 days post administration of 10-HOME (**Fig. 5B**).

180   Other subtypes of CD4+ T cells (Th2) didn't exhibit any statistically significant increase in

181   abundance **(Fig. 5C)**.

182

Discussion

184   Biofilm formation enables single-cell microbes to assume a temporary multicellular lifestyle, in

185   which "group behavior" facilitates survival in adverse environments[31]. The transition from

186   planktonic growth (associated with acute pathogenic infections) to biofilm occurs in response to

187   environmental changes, and involves multiple regulatory networks thereby mediating the spatial

188   and temporal reorganization of the bacterial cell[31]. Bacterial biofilms have been implicated to

189   cause gastric cancer by *Helicobacter pylori*[32], colon cancer[33, 34], breast implant-associated

190   anaplastic large cell lymphoma (BIA-ALCL) and chronic inflammation[35-37]. The factors that involve

191   interplay between host and pathogen are influenced by the micro-environmental niche where the

192   bacteria reside[22, 38, 39]. Breast implants provided a conducive surface for the adherence and growth

193   of bacterial biofilms[40]. The breast is a modified sweat gland, with multiple external opening from

194   the mammary ducts *via* the nipple, providing a passage for microbes (normal skin flora) to the

195   breast tissue. This concept has been supported by a report whereby researchers have shown the

196   presence of microbes deep inside the breast tissue[41]. Many bacteria belonging to the normal

197   microflora of the body have been reported to form bacterial biofilms[42]. *Pseudomonas*

198   *aeruginosa*[43, 44], *Staphylococcus aureus* [45] and *Ralstonia picketii* [40, 46] are some of the common

199   biofilm forming species associated with breast implants. The bacterial biofilms are difficult to

200   detect since they have subdued metabolism and may not be detectable as CFUs in standard

201   microbiological assays [21, 22]. They can be identified through structural assays like scanning

202   electron microscopy (SEM)[22, 47] and genetic assays (e.g.,16S rRNA sequencing)[48]. The

203   observation in this study of increased abundance of bacterial biofilm comprised of *Staphylococcus*

204   *epidermidis* associated with implant-associated tissue of BII patients relative to controls was thus

205   critical in understanding to the potential pathology of BII. It is to be noted that while this study was

206   being performed, anecdotal evidence of *S.epidermidis* with BII was reported by Mark *et al* [49] .

207   The oxidation of fatty acids is one of the main biochemical reactions in the synthesis of lipid

208   mediators. The oxygenation of unsaturated fatty acids leads to the formation of oxylipins, although

209   free fatty acids are not readily available as they are found as triglycerides. The action of bacterial

210   lipases, such as dioxygenases (DOX) and lipoxygenases (LOX) on breast adipose result in the

211   availability of free fatty acids. When oleic acid is used as a bacterial substrate, it is oxidized to

212   form 10-HOME. The unique adipose tissue found in breast tissue is rich in oleic acid containing

213   lipids[50, 51]. The oxylipin 10-HOME has been reported to promote bacterial biofilms *in vitro*[24]. The

214   increased abundance of 10-HOME in our study associated with breast tissues of BII subjects thus

215   provides evidence that breast microflora may interact with breast lipids promoting the formation

216   of bacterial biofilms.

217   Oxylipins are also known to be immune-modulatory. It has been reported that 12,13 DiHOME

218   derived from oxidation of linoleic acid led to the reduction of regulatory T cells (Tregs), impeded

219   immune tolerance and promoted childhood atopy and asthma[25]. Elevated levels of 10-HOME

220   formed due to bacterial biofilms could lead to immune cell activation. Reports suggest that CD4^{+}

221   T cells are activated due to the persistent presence of a bacterial biofilm[52, 53]. CD4^{+} T cells play

222   an important role in the pathogenesis of chronic systemic inflammatory autoimmune diseases

223   such as multiple sclerosis, diabetes and rheumatoid arthritis[54-56]. CD4^{+} T cells can be divided into

224   Th1, Th2, Th9, Th17 and Th22 subsets based upon the cytokines they produce. In chronic

225   inflammatory systemic autoimmune diseases such as diabetes, multiple sclerosis and rheumatoid

226   arthritis, Th1 cells were found to be involved[57]. It is to be noted that many of the symptoms of BII

227   patients were similar to rheumatoid arthritis and multiple sclerosis[8]. Th1 cells trigger delayed type

228   hypersensitivity (DTH) reactions (which are mostly mediated by macrophages) and

229   immunoglobulin class switch towards IgG2a[55, 56].

230   Oxidized lipids have been associated with pain and inflammatory conditions[58]. Pain reported as

231   arthralgia and myalgia are common in BII. We identified increased presence of CD4^{+} Th1 cells

232   in the breast tissue and peripheral blood of BII subjects. Findings of this study demonstrate that

233   10-HOME was capable of polarizing naïve CD4^{+} T cells towards Th1 subtype *in vitro*. Increased

234   abundance of transcription factor T-BET required for Th1 fate was identified post 10-HOME

235   treatment. The polarization to Th1 subtype was also supported by the observation of increased

236   expression of pro-inflammatory cytokine IFN-γ secreted by Th1 cells. Systemic analyses in our

237   study didn't revealed polarization towards Th2, Th9 and Th22 subtypes. It is to be noted that the

238   current work does not rule out the polarization of naïve CD4^{+} T cells to Th17 subtype upon

239   treatment with 10-HOME. Th17 subtype has been also reported to be associated with auto-

240   immune syndrome[59].

241   To correlate the association of 10-HOME with activation of CD4$^+$ T cells *in vivo*, mice were

242   administered with 10-HOME in their mammary fat pad. An increased abundance of CD4$^+$ Th1

243   cells in peripheral circulation in 10-HOME administered mice was observed. These observations

244   also help to explain the increased abundance CD4$^+$ Th1 in the BII subjects.

245   Taken together, we investigated the biofilm hypothesis of breast implant illness through a host-

246   pathogen interaction. The breast microenvironment led to formation of biofilm derived 10-HOME

247   from host oleic acid. The 10-HOME thus formed led to activation of CD4$^+$ Th1 cells *in vitro* and *in*

248   *vivo*. The study provides the first evidence of a possible link of biofilm derived 10-HOME inducing

249   an autoimmune response in patients with BII. Additionally, in light of reports of biofilm association

250   with metal implants such as orthopedic arthroplasty, this study provides an explanation of

251   autoimmune responses reported using those metal implants[16-20]. The findings of this study

252   suggest that management of biofilm can help to increase the safety and long-term use of implants.

253   Further research needs to be conducted to elucidate if other biofilm forming bacterial species are

254   involved in the pathogenesis of BII. Also, more investigation is warranted to decipher the pathway

255   leading to the onset of BII post-biofilm formation and the involvement of other biofilm derived

256   metabolites.

257

Materials and Methods

259   **Human subjects.** Subjects participating in the study were patients diagnosed with BII.

260   Demographic characteristics of patients presented in **(Supplementary Table 2)**. All human

261   studies were approved by The Indiana University School of Medicine Institutional Review Board.

262   Declaration of Helsinki protocols was followed, and patients gave their written informed consent.

263   **Animals.** All animal (mice) experiments were approved by the Indiana University School of

264   Medicine Institutional Animal Care and Use Committee (SoM-IACUC) under protocol 19102 -

265   Murine model of breast implant diseases. Animals were housed under a 12-h light–dark cycle with

266   food and water *ad libitum*.

267   **Bacterial strains**. Staphylococcus epidermidis (Winslow and Winslow) Evans (ATCC® 35984™)

268   were grown on tryptic soy agar plate at 37°C.

269   **Scanning Electron Microscope Imaging**. The samples were collected in glutaraldehyde fixation

270   buffer, dehydrated with graded ethanol, and treated with hexamethyldisilazane (HMDS, Ted Pella

271   Inc.) and left overnight for drying[22, 38]. Before scanning, samples were mounted and coated with

272   gold. Samples were imaged with FEI™ NOVA nanoSEM scanning electron microscope (FEI™,

273   Hillsboro, OR) equipped with a field-emission gun electron source.

274   **Wheat-germ agglutinin (WGA) staining.** Paraffin embedded capsules surrounding the implant

275   were sectioned on the slide. Wheat Germ Agglutinin, Alexa Fluor™ 488 Conjugate (Invitrogen)

276   stock solution (1mg/ml) was diluted in PBS. The sections were stained with Wheat Germ

277   Agglutinin (dilution 1:200) for 10 mins [60]. The slides were then mounted and imaged on a Zeiss

278   LSM 880 microscope equipped with the AIRYscan detector.

279   **NGS sequencing for 16S rRNA**. Microbial DNA in each sample were sequenced by MicrogenDx

280   Inc using the Illumina MiSeq sequencer. Forward and reverse primers were used to detect and

281   amplify the target sequence, for 16S gene in bacteria. The samples are differentiated from each

282   other when run on the MiSeq sequencer by a "tag," a unique identifying sequence attached to the

283   forward and reverse primers implemented when the targeted sequence is amplified using PCR.

284   Following PCR, purification of the pooled DNA was done by removing small fragments using both

285   Agencourt Ampure beads and Qiagen Minelute kit. The DNA was quantified and prepared for

286   sequencing. Finally, the DNA library was run on the MiSeq sequencer. The sequencing reads

287   were analyzed for quality and length during the data analysis. The data analysis pipeline

288   consisted of two major stages, the denoising and chimera detection stage and the microbial

289   diversity analysis stage. During the denoising and chimera detection stage, denoising was

290   performed using various techniques to remove short sequences, singleton sequences, and noisy

291   reads. With the low-quality reads removed, chimera detection was performed to aid in the removal

292   of chimeric sequences. The high-quality sequencing reads of the variable region of 16S rRNA

293   were compared to curated database of MicrogenDx. The database is comprised of 18500 unique

294   bacteria.

295   **Synthesis of 10-HOME.** For the synthesis of 10-HOME, a convergent Horner-Wadsworth-

296   Emmons approach was employed. Indiana University has filed a provisional patent application

297   (Application # 63/107,626) on behalf of REM, IK and MS relating to the methods and synthesis of

298   10-HOME and its deuterated 17,17,18,18,18 d_5 analog to be used as analytical standards.

299   **Primary T-cell isolation.** Naïve CD4$^+$ T cells were isolated from peripheral blood mononuclear

300   cells (PBMC). Briefly, PBMCs were isolated by Ficoll-Paque PLUS density gradient

301   sedimentation. Naïve CD4$^+$ T cells were then enriched using immunomagnetic, column-free,

302   negative selection (Naïve CD4 T cell isolation kit, Miltenyi Biotec)[61]. Unwanted cells (CD8, CD14,

303   CD15, CD16, CD19, CD25, CD34, CD36, CD45RO, CD56, CD123, TCRγ/δ, HLA-DR, and

304   CD235a (Glycophorin A)) were removed using antibody complexes recognizing non-naïve CD4

305   T cells and dextran-coated magnetic particles.

306   **Primary CD4$^+$ T cell culture and 10-HOME treatment.** Primary CD4$^+$ T cells were cultured under

307   standard conditions at 37°C in a humidified incubator with 5% CO_2 in RPMI-1640 growth medium

308   supplemented with 10% FBS, 100 IU/ml penicillin, 0.1 mg/ml streptomycin, 10 mmol/l L-glutamine

309   supplemented with IL2 for 48h[62]. Following that, CD4^{+} T cells were treated with oxylipin 10-HOME

310   (100 μM) or vehicle control for 48 h.

311   **Immunohistochemistry and immunocytochemistry**. Paraffin embedded breast tissue blocks

312   were sectioned, deparaffinized and immunostained[22, 39, 63]. Immunohistochemical staining of the

313   sections were performed using standard procedures using the following primary antibodies: α-

314   CD4 antibody (abcam# ab133616; dilution 1:200), α-CD36 antibody (Abcam # ab80080, clone

315   MF3, dilution: 1:200), α- T-bet antibody (Abcam # ab91109, clone 4B10, dilution: 1:200). To

316   enable fluorescence detection, sections were incubated with appropriate Alexa Fluor® 488

317   (green, Molecular probes), or Alexa Fluor® 564 (red, Molecular probes) conjugated secondary

318   antibodies. The sections were counterstained with DAPI (Sigma). For immunocytochemistry, cells

319   were fixed with IC fixation buffer (eBioscience), blocked with 10 percent normal goat serum

320   (Vector Laboratories), incubated with primary and secondary antibodies and counterstained with

321   DAPI. Mosaic images were collected using a Zeiss Axiovert 200 M, inverted fluorescence

322   microscopy or confocal microscopy (LSM880). Image analysis was performed using Zen

323   (Zeiss) software to quantitate fluorescence intensity (fluorescent pixels).

324   **Lipid extraction and 10-HOME quantification using LCMS**. LC-MS/MS targeted analysis from

325   capsule and breast adipose tissue was performed. Samples were weighed and transferred to 2

326   ml vials with 1.4 mm ceramic beads and 1 ml of water with 0.1% formic acid. The standard solution

327   was prepared by aliquoting 1μl of each stock solution into a new tube drying the original solvent

328   and solubilizing in 1 ml of 100% ethanol to obtain a final concentration of 1 ng/ml each. Samples

329   were homogenized using Precellys24 tissue homogenizer (Bertin Technologies, Rockville, MD).

330   The total volume of the homogenate was extracted with ethyl acetate in a 1:1 volume ratio.

331   Samples were vortexed for 1 minute and centrifuged at 14.000 rpm for 10 minutes. The organic

332   phase was collected and transferred to a new vial to be evaporated and stored at -80°C until

333   analysis. The dried lipid extracts were reconstituted with 50 μl of methanol/water at 1:1 volume

334   ratio and submitted for targeted quantification by liquid chromatography tandem MS (LC/MS/MS).

335   The LC column used was an Acquity UPLC BEH C18 1.7µm particle size - 2.1x100 mm (Waters,

336   Milford, MA). The binary pump flow rate was set at 0.3mL/min in an Agilent UPLC (G7120A) using

337   water and 0.1% formic acid as mobile phase A and acetonitrile and 0.1% formic acid as mobile

338   phase B. The LC column was pre-equilibrated with 80% A for 1 min. The binary pump was set in

339   a linear gradient to 100% B in 8 min and held for 2.50 min. It was then returned to 80% A and re-

340   equilibrated for 4 min. Ten µL of the reconstituted sample was delivered to the column through a

341   multisampler (G7167B) into a QQQ6470A triple quadrupole mass spectrometer (Agilent

342   Technologies, San Jose, CA) equipped with ESI Jet Stream ion source. In the mass spectrometer

343   the capillary voltage was 3500 V on the negative ion mode, the gas temperature was 325ºC, gas

344   flow was set at 8l/min, the sheath gas heater at 250ºC and the sheath gas flow at 7 l/min. The

345   fragmentation voltage was 100 and the cell accelerator voltage was 4 V. The MRMs (parent-

346   fragment) for the acquisition included were 297.5->155.4 for 10-HOME and for the internal

347   standard it was 302.4->155.4. Concentrations in ng/mg of tissue were obtained by normalizing by

348   the dried weight of the sample homogenized and by the concentration of the deuterated internal

349   standard. To quantify 10-HOME, calibration curves were done with 7 serial dilutions of the stock

350   solution starting at 10 ng as the highest concentration. Data processing was carried out by using

351   Mass Hunter (B.06.00) using software Quant and Qual.

352   **Flow cytometry analyses.** The fluorescence and light-scattering properties (forward scatter and

353   side scatter) of the cells were determined by using BD Accuri C6. Signals from cells labeled with

354   conjugated fluorophores were detected. The following antibodies were used for different flow

355   cytometry analysis. PE anti-human CD183 (CXCR3) (clone G025H7, Biolegend # 353705, 2

356   µg/ml), PE anti-human CD194 (CCR4) (clone L291H4, Biolegend # 359412, 0.5 µg/ml), PE anti-

357   human CD196 (CCR6) (clone G034E3, Biolegend # 353410, 0.5 µg/ml), FITC anti-human CD4

358   (clone A161A1, Biolegend # 357406 , 0.5 µg/ml), APC anti-human CD194 (CCR4) (clone L291H4,

359   Biolegend # 359407, 0.5 µg/ml), Alexa Fluor® 700 anti-human CD196 (CCR6) (clone G034E3,

360   Biolegend # 353433, 0.5 µg/ml), PE anti-human CD36 (clone 5-271, Biolegend # 336205, 1

361   µg/ml), FITC anti-mouse CD4 (clone GK1.5, Biolegend # 100406, 0.5 µg/ml), APC anti-mouse

362   CD36 (clone HM36, Biolegend # 102612, 0.5 µg/ml), PE anti-mouse CD183 CD36 (clone CXCR3-

363   173, Biolegend # 126506, 0.5 µg/ml), PE anti-mouse CD196 (clone 29-2L17, Biolegend # 129804,

364   0.5 µg/ml), APC anti-mouse CD194 (clone 2G12, Biolegend # 131211, 0.5 µg/ml), PE anti-mouse

365   FOXP3 (clone MF14, Biolegend # 126403, 0.5 µg/ml), PE anti-T-bet Antibody (clone 4B10,

366   Biolegend # 644809, 0.5 µg/ml). For intracellular markers, TBET and GATA3 permeabilization

367   was performed through True-nuclear transcription factor buffer set (Biolegend # 424401). Auto

368   compensation was performed using samples stained with single flurophores. Gates were set

369   manually. BD Diva (BD Biosciences), and FlowJo softwares were used for analyses[63].

370   Logarithmic scale was used to measure cell fluorescence. Appropriate IgG control fluorescence

371   compensation was applied to avoid false positive signals.

372   **ELISA**. Cell-free supernatants were collected and stored at −80°C. ELISAs for IFN-γ, IL4 and

373   IL10 were performed using DuoSet kits (R&D Systems) as per manufacturer's protocol.

374   **10-HOME administration in mice**. At approximately 9 to 10 weeks of age, female mice were

375   anesthetized with isoflurane, and five injections of 10-HOME (15 mg/kg body weight) every

376   alternate day was made with a 27 G needle to the abdominal mammary fat pad of mice. Post-two

377   weeks of the dose the mice were euthanized. Blood, mammary fat pad and spleen were harvested

378   for subsequent analyses.

379   **Quantitative RT PCR**. Breast tissue was pulverized using tissue pulverizer (6770 Freezer/Mill)

380   and total RNA was extracted using miRVana (Thermo Fisher Scientific). cDNA was made using

381   SuperScript™ III First-Strand Synthesis System (Invitrogen) or SuperScript™ VILO™ cDNA

382   Synthesis Kit (Invitrogen). Quantitative or real-time PCR (Sybr Green) approach was used for

383   mRNA quantification [63-68]. Primer sequences used in this study provided in (**Supplementary**

384   **Table 3**).

385

386   **Quantification and statistical analysis**

387   The data analysis was performed using student's t-test (two-tailed) to determine significant

388   differences. Mean, standard deviation and student paired *t*-test analysis was done using in-built

389   function in Microsoft Excel 2010. Data are presented as mean ± SEM (*in vivo*) or ± SD (*in vitro*)

390   as reported in figure legends. Comparisons among multiple groups were tested using ANOVA in-

391   built function in GraphPad Prism 8.4.2. $p<0.05$ was considered statistically significant.

392   **ACKNOWLEDGEMENTS**

402   **AUTHOR CONTRIBUTIONS**

403   MS, IK, and AHH conceived and designed the work. IK, REM, CKP, BWV, CRN, LS, KS, ML, JVD

404   participated in the data acquisition. MS, REM, IK, CKP, AHH and MEK wrote the manuscript. MS,

405   REM, CKS, GMG, MEK, BWV reviewed the manuscript.

DECLARATION OF INTERESTS

The authors declare no competing interests

REFERENCES

1.   Safety of Silicone Breast Implants. In: S. Bondurant, V. Ernster and R. Herdman, eds. *Institute of Medicine* Washington (DC): The National Academies Press; 1999(https://doi.org/10.17226/9602).

2.   FDA Update on the Safety of Silicone Gel-Filled Breast Implants. 2011;https://www.fda.gov/media/80685/download.

3.   2019 Plastic Surgery Statistics. 2019;https://www.plasticsurgery.org/news/plastic-surgery-statistics.

4.   Fryzek JP, Signorello LB, Hakelius L, Feltelius N, Ringberg A, Blot WJ, McLaughlin JK and Nyren O. Self-reported symptoms among women after cosmetic breast implant and breast reduction surgery. *Plast Reconstr Surg*. 2001;107:206-13.

5.   Maijers MC, de Blok CJ, Niessen FB, van der Veldt AA, Ritt MJ, Winters HA, Kramer MH and Nanayakkara PW. Women with silicone breast implants and unexplained systemic symptoms: a descriptive cohort study. *Neth J Med*. 2013;71:534-40.

6.   ASAPS. Breast Implant Illness - Frequently Asked Questions/Talking Points. *https://wwwsurgeryorg/sites/default/files/BreastImplantIllness_8-21-2019_FINALpdf*. 2019.

7.   Balk EM, Earley A, Avendano EA and Raman G. Long-Term Health Outcomes in Women With Silicone Gel Breast Implants: A Systematic Review. *Ann Intern Med*. 2016;164:164-75.

8.   Coroneos CJ, Selber JC, Offodile AC, 2nd, Butler CE and Clemens MW. US FDA Breast Implant Postapproval Studies: Long-term Outcomes in 99,993 Patients. *Ann Surg*. 2019;269:30-36.

430   9.   Khoo T, Proudman S and Limaye V. Silicone breast implants and depression,

431   fibromyalgia and chronic fatigue syndrome in a rheumatology clinic population. *Clin Rheumatol*.

432   2019;38:1271-1276.

433   10.   Lee IM, Cook NR, Shadick NA, Pereira E and Buring JE. Prospective cohort study of

434   breast implants and the risk of connective-tissue diseases. *Int J Epidemiol*. 2011;40:230-8.

435   11.   Singh N, Picha GJ, Hardas B, Schumacher A and Murphy DK. Five-Year Safety Data for

436   More than 55,000 Subjects following Breast Implantation: Comparison of Rare Adverse Event

437   Rates with Silicone Implants versus National Norms and Saline Implants. *Plast Reconstr Surg*.

438   2017;140:666-679.

439   12.   Watad A, Rosenberg V, Tiosano S, Cohen Tervaert JW, Yavne Y, Shoenfeld Y, Shalev

440   V, Chodick G and Amital H. Silicone breast implants and the risk of autoimmune/rheumatic

441   disorders: a real-world analysis. *Int J Epidemiol*. 2018;47:1846-1854.

442   13.   de Boer M, Colaris M, van der Hulst R and Cohen Tervaert JW. Is explantation of

443   silicone breast implants useful in patients with complaints? *Immunol Res*. 2017;65:25-36.

444   14.   Peters W, Smith D, Fornasier V, Lugowski S and Ibanez D. An outcome analysis of 100

445   women after explantation of silicone gel breast implants. *Ann Plast Surg*. 1997;39:9-19.

446   15.   Tanne JH. FDA approves silicone breast implants 14 years after their withdrawal. *BMJ*.

447   2006;333:1139.

448   16.   Alijotas-Reig J, Esteve-Valverde E, Gil-Aliberas N and Garcia-Gimenez V.

449   Autoimmune/inflammatory syndrome induced by adjuvants-ASIA-related to biomaterials:

450   analysis of 45 cases and comprehensive review of the literature. *Immunol Res*. 2018;66:120-

451   140.

452   17.   Greenland S and Finkle WD. A case-control study of prosthetic implants and selected

453   chronic diseases in Medicare claims data. *Ann Epidemiol*. 1998;8:319-26.

454   18.   Laing TJ, Schottenfeld D, Lacey JV, Jr., Gillespie BW, Garabrant DH, Cooper BC,

455   Heeringa SG, Alcser KH and Mayes MD. Potential risk factors for undifferentiated connective

456   tissue disease among women: implanted medical devices. *Am J Epidemiol*. 2001;154:610-7.

457   19.   Mellemkjaer L, Friis S, McLaughlin JK, Thomsen BL, Kjoller K, Hogsted C, Winther JF,

458   Blot WJ and Olsen JH. Connective tissue disease after hip and knee implant surgery. *Scand J*

459   *Rheumatol*. 2001;30:82-6.

460   20.   Signorello LB, Ye W, Fryzek JP, Blot WJ, Lipworth L, McLaughlin JK and Nyren O. A

461   nationwide followup study of autoimmune and connective tissue disease among hip and knee

462   implant patients. *J Long Term Eff Med Implants*. 2002;12:255-62.

463   21.   Vyas KS and Wong LK. Detection of Biofilm in Wounds as an Early Indicator for Risk for

464   Tissue Infection and Wound Chronicity. *Ann Plast Surg*. 2016;76:127-31.

465   22.   Roy S, Elgharably H, Sinha M, Ganesh K, Chaney S, Mann E, Miller C, Khanna S,

466   Bergdall VK, Powell HM, Cook CH, Gordillo GM, Wozniak DJ and Sen CK. Mixed-species

467   biofilm compromises wound healing by disrupting epidermal barrier function. *J Pathol*.

468   2014;233:331-343.

469   23.   Rhoads DD, Cox SB, Rees EJ, Sun Y and Wolcott RD. Clinical identification of bacteria

470   in human chronic wound infections: culturing vs. 16S ribosomal DNA sequencing. *BMC Infect*

471   *Dis*. 2012;12:321.

472   24.   Martinez E and Campos-Gomez J. Oxylipins produced by Pseudomonas aeruginosa

473   promote biofilm formation and virulence. *Nat Commun*. 2016;7:13823.

474   25.   Levan SR, Stamnes KA, Lin DL, Fujimura KE, Ownby DR, Zoratti EM, Boushey HA,

475   Johnson CC and Lynch SV. Neonatal gut-microbiome-derived 12,13 DiHOME impedes

476   tolerance and promotes childhood atopy and asthma. *bioRxiv*. 2018:311704.

477   26.   Kanhere A, Hertweck A, Bhatia U, Gokmen MR, Perucha E, Jackson I, Lord GM and

478   Jenner RG. T-bet and GATA3 orchestrate Th1 and Th2 differentiation through lineage-specific

479   targeting of distal regulatory elements. *Nat Commun*. 2012;3:1268.

480   27.   Skapenko A, Leipe J, Lipsky PE and Schulze-Koops H. The role of the T cell in

481   autoimmune inflammation. *Arthritis Research & Therapy*. 2005;7:S4.

482   28.   Zhang X, Fitzsimmons RL, Cleland LG, Ey PL, Zannettino AC, Farmer EA, Sincock P

483   and Mayrhofer G. CD36/fatty acid translocase in rats: distribution, isolation from hepatocytes,

484   and comparison with the scavenger receptor SR-B1. *Lab Invest*. 2003;83:317-32.

485   29.   Perera LP, Zhang M, Nakagawa M, Petrus MN, Maeda M, Kadin ME, Waldmann TA and

486   Perera PY. Chimeric antigen receptor modified T cells that target chemokine receptor CCR4 as

487   a therapeutic modality for T-cell malignancies. *Am J Hematol*. 2017;92:892-901.

488   30.   Oishi N, Hundal T, Phillips JL, Dasari S, Hu G, Viswanatha DS, He R, Mai M, Jacobs

489   HK, Ahmed NH, Syrbu SI, Salama Y, Chapman JR, Vega F, Sidhu J, Bennani NN, Epstein AL,

490   Medeiros LJ, Clemens MW, Miranda RN and Feldman AL. Molecular profiling reveals a hypoxia

491   signature in breast implant-associated anaplastic large cell lymphoma. *Haematologica*. 2020.

492   31.   Kostakioti M, Hadjifrangiskou M and Hultgren SJ. Bacterial biofilms: development,

493   dispersal, and therapeutic strategies in the dawn of the postantibiotic era. *Cold Spring Harb*

494   *Perspect Med*. 2013;3:a010306.

495   32.   Parsonnet J. Bacterial infection as a cause of cancer. *Environ Health Perspect*.

496   1995;103 Suppl 8:263-8.

497   33.   Mousa JJ, Yang Y, Tomkovich S, Shima A, Newsome RC, Tripathi P, Oswald E, Bruner

498   SD and Jobin C. MATE transport of the E. coli-derived genotoxin colibactin. *Nat Microbiol*.

499   2016;1:15009.

500   34.   Tomkovich S, Yang Y, Winglee K, Gauthier J, Muhlbauer M, Sun X, Mohamadzadeh M,

501   Liu X, Martin P, Wang GP, Oswald E, Fodor AA and Jobin C. Locoregional Effects of Microbiota

502   in a Preclinical Model of Colon Carcinogenesis. *Cancer Res*. 2017;77:2620-2632.

503   35.   Cappelli G, Tetta C and Canaud B. Is biofilm a cause of silent chronic inflammation in

504   haemodialysis patients? A fascinating working hypothesis. *Nephrol Dial Transplant*.

505   2005;20:266-70.

506   36.   Zhao G, Usui ML, Lippman SI, James GA, Stewart PS, Fleckman P and Olerud JE.

507   Biofilms and Inflammation in Chronic Wounds. *Adv Wound Care (New Rochelle)*. 2013;2:389-

508   399.

509   37.   Hu H, Johani K, Almatroudi A, Vickery K, Van Natta B, Kadin ME, Brody G, Clemens M,

510   Cheah CY, Lade S, Joshi PA, Prince HM and Deva AK. Bacterial Biofilm Infection Detected in

511   Breast Implant-Associated Anaplastic Large-Cell Lymphoma. *Plast Reconstr Surg*.

512   2016;137:1659-69.

513   38.   Barki KG, Das A, Dixith S, Ghatak PD, Mathew-Steiner S, Schwab E, Khanna S,

514   Wozniak DJ, Roy S and Sen CK. Electric Field Based Dressing Disrupts Mixed-Species

515   Bacterial Biofilm Infection and Restores Functional Wound Healing. *Ann Surg*. 2019;269:756-

516   766.

517   39.   Roy S, Santra S, Das A, Dixith S, Sinha M, Ghatak S, Ghosh N, Banerjee P, Khanna S,

518   Mathew-Steiner S, Ghatak PD, Blackstone BN, Powell HM, Bergdall VK, Wozniak DJ and Sen

519   CK. Staphylococcus aureus Biofilm Infection Compromises Wound Healing by Causing

520   Deficiencies in Granulation Tissue Collagen. *Ann Surg*. 2020;271:1174-1185.

521   40.   James GA, Boegli L, Hancock J, Bowersock L, Parker A and Kinney BM. Bacterial

522   Adhesion and Biofilm Formation on Textured Breast Implant Shell Materials. *Aesthetic Plast*

523   *Surg*. 2019;43:490-497.

524   41.   Urbaniak C, Cummins J, Brackstone M, Macklaim JM, Gloor GB, Baban CK, Scott L,

525   O'Hanlon DM, Burton JP, Francis KP, Tangney M and Reid G. Microbiota of human breast

526   tissue. *Appl Environ Microbiol*. 2014;80:3007-14.

527   42.   Brandwein M, Steinberg D and Meshner S. Microbial biofilms and the human skin

528   microbiome. *NPJ Biofilms Microbiomes*. 2016;2:3.

529   43.   Cohen JB, Carroll C, Tenenbaum MM and Myckatyn TM. Breast Implant-Associated

530   Infections: The Role of the National Surgical Quality Improvement Program and the Local

531   Microbiome. *Plast Reconstr Surg*. 2015;136:921-9.

532   44.   Walker JN, Poppler LH, Pinkner CL, Hultgren SJ and Myckatyn TM. Establishment and

533   Characterization of Bacterial Infection of Breast Implants in a Murine Model. *Aesthet Surg J*.

534   2020;40:516-528.

535   45.   Song JH, Kim YS, Jung BK, Lee DW, Song SY, Roh TS and Lew DH. Salvage of

536   Infected Breast Implants. *Arch Plast Surg*. 2017;44:516-522.

537   46.   Brindle CT, Porter S, Bijlani K, Arumugam S, Matias R, Najafi R and Fisher J.

538   Preliminary Results of the Use of a Stabilized Hypochlorous Acid Solution in the Management of

539   Ralstonia Pickettii Biofilm on Silicone Breast Implants. *Aesthet Surg J*. 2018;38:S52-S61.

540   47.   Azeredo J, Azevedo NF, Briandet R, Cerca N, Coenye T, Costa AR, Desvaux M, Di

541   Bonaventura G, Hebraud M, Jaglic Z, Kacaniova M, Knochel S, Lourenco A, Mergulhao F,

542   Meyer RL, Nychas G, Simoes M, Tresse O and Sternberg C. Critical review on biofilm methods.

543   *Crit Rev Microbiol*. 2017;43:313-351.

544   48.   Swearingen MC, DiBartola AC, Dusane D, Granger J and Stoodley P. 16S rRNA

545   analysis provides evidence of biofilms on all components of three infected periprosthetic knees

546   including permanent braided suture. *Pathog Dis*. 2016;74.

547   49.   Lee M, Ponraja G, McLeod K and Chong S. Breast Implant Illness: A Biofilm Hypothesis.

548   *Plast Reconstr Surg Glob Open*. 2020;8:e2755.

549   50.   Chajes V, Niyongabo T, Lanson M, Fignon A, Couet C and Bougnoux P. Fatty-acid

550   composition of breast and iliac adipose tissue in breast-cancer patients. *Int J Cancer*.

551   1992;50:405-8.

552   51.   Zhu ZR, Agren J, Mannisto S, Pietinen P, Eskelinen M, Syrjanen K and Uusitupa M.

553   Fatty acid composition of breast adipose tissue in breast cancer patients and in patients with

554   benign breast disease. *Nutr Cancer*. 1995;24:151-60.

555   52.   Kotsougiani D, Pioch M, Prior B, Heppert V, Hansch GM and Wagner C. Activation of T

556   Lymphocytes in Response to Persistent Bacterial Infection: Induction of CD11b and of Toll-Like

557   Receptors on T Cells. *Int J Inflam*. 2010;2010:526740.

558   53.   Gonzalez JF, Hahn MM and Gunn JS. Chronic biofilm-based infections: skewing of the

559   immune response. *Pathog Dis*. 2018;76.

560   54.   Steinman L. A few autoreactive cells in an autoimmune infiltrate control a vast population

561   of nonspecific cells: a tale of smart bombs and the infantry. *Proc Natl Acad Sci U S A*.

562   1996;93:2253-6.

563   55.   Nicholson LB and Kuchroo VK. Manipulation of the Th1/Th2 balance in autoimmune

564   disease. *Curr Opin Immunol*. 1996;8:837-42.

565   56.   Liblau RS, Singer SM and McDevitt HO. Th1 and Th2 CD4+ T cells in the pathogenesis

566   of organ-specific autoimmune diseases. *Immunol Today*. 1995;16:34-8.

567   57.   Raphael I, Nalawade S, Eagar TN and Forsthuber TG. T cell subsets and their signature

568   cytokines in autoimmune and inflammatory diseases. *Cytokine*. 2015;74:5-17.

569   58.   Osthues T and Sisignano M. Oxidized Lipids in Persistent Pain States. *Front Pharmacol*.

570   2019;10:1147.

571   59.   Tabarkiewicz J, Pogoda K, Karczmarczyk A, Pozarowski P and Giannopoulos K. The

572   Role of IL-17 and Th17 Lymphocytes in Autoimmune Diseases. *Arch Immunol Ther Exp*

573   *(Warsz)*. 2015;63:435-49.

574   60.   Deng B, Ghatak S, Sarkar S, Singh K, Das Ghatak P, Mathew-Steiner SS, Roy S,

575   Khanna S, Wozniak DJ, McComb DW and Sen CK. Novel Bacterial Diversity and Fragmented

576   eDNA Identified in Hyperbiofilm-Forming Pseudomonas aeruginosa Rugose Small Colony

577   Variant. *iScience*. 2020;23:100827.

578   61.   Shen W, Falahati R, Stark R, Leitenberg D and Ladisch S. Modulation of CD4 Th cell

579   differentiation by ganglioside GD1a in vitro. *J Immunol*. 2005;175:4927-34.

580   62.   Ganusov VV, Milutinovic D and De Boer RJ. IL-2 regulates expansion of CD4+ T cell

581   populations by affecting cell death: insights from modeling CFSE data. *J Immunol*.

582   2007;179:950-7.

583   63.   Sinha M, Sen CK, Singh K, Das A, Ghatak S, Rhea B, Blackstone B, Powell HM,

584   Khanna S and Roy S. Direct conversion of injury-site myeloid cells to fibroblast-like cells of

585   granulation tissue. *Nat Commun*. 2018;9:936.

586   64.   Das A, Ganesh K, Khanna S, Sen CK and Roy S. Engulfment of apoptotic cells by

587   macrophages: a role of microRNA-21 in the resolution of wound inflammation. *J Immunol*.

588   2014;192:1120-9.

589   65.   Das A, Ghatak S, Sinha M, Chaffee S, Ahmed NS, Parinandi NL, Wohleb ES, Sheridan

590   JF, Sen CK and Roy S. Correction of MFG-E8 Resolves Inflammation and Promotes Cutaneous

591   Wound Healing in Diabetes. *J Immunol*. 2016;196:5089-100.

592   66.   Ganesh K, Das A, Dickerson R, Khanna S, Parinandi NL, Gordillo GM, Sen CK and Roy

593   S. Prostaglandin E(2) induces oncostatin M expression in human chronic wound macrophages

594   through Axl receptor tyrosine kinase pathway. *J Immunol*. 2012;189:2563-73.

595   67.   Khanna S, Biswas S, Shang Y, Collard E, Azad A, Kauh C, Bhasker V, Gordillo GM, Sen

596   CK and Roy S. Macrophage dysfunction impairs resolution of inflammation in the wounds of

597   diabetic mice. *PLoS One*. 2010;5:e9539.

598   68.   Das A, Datta S, Roche E, Chaffee S, Jose E, Shi L, Grover K, Khanna S, Sen CK and

599   Roy S. Novel mechanisms of Collagenase Santyl Ointment (CSO) in wound macrophage

600   polarization and resolution of wound inflammation. *Sci Rep*. 2018;8:1696.

601

602

603

604

605
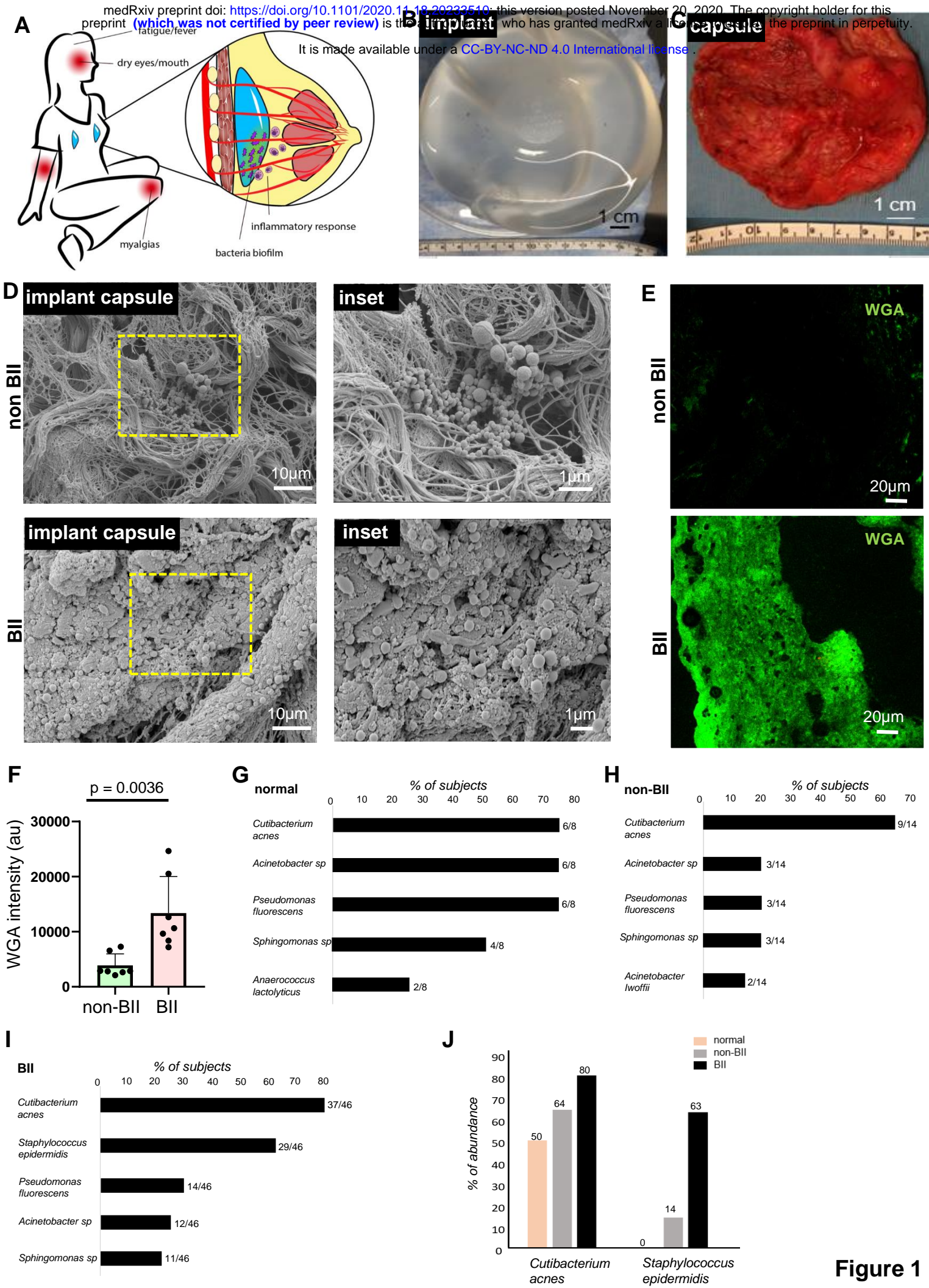
Figure 1

Figure 1. Bacterial Biofilm in Implant-Associated with BII

(A) Schematic presentation of the bacterial biofilm association with breast implant illness (BII)

(B) Breast implant isolated from a subject

(C) Capsule associated with breast implant of the subject shown in (B)

(D) Increased abundance of bacterial biofilm from the implant-associated capsule of BII compared to non BII subjects as determined through scanning electron microscopy. Zoomed insets of region of interest (ROI) dotted yellow square shown. n=10 non-BII subjects, n=25 BII subjects.

(E-F) E, Increased abundance of bacterial biofilm as measured through wheat germ agglutinin (WGA) assay in the capsules of BII subjects compared to the non-BII capsules. **F**, quantification of biofilm aggregates using WGA staining. Data presented as mean ± SEM, n=7 non-BII, n=7 BII

(G-I) 16S rRNA NGS based bacterial typing from the breast tissues of **G**, normal; **H**, non-BII and **I**, BII subjects. Top five bacterial species in each group represented. Absolute values of subject samples associated with a bacterial species is provided in parenthesis n=8 (normal), n=14 (non-BII), n=46 (BII)

(J) Increased abundance of biofilm forming *Staphylococcus epidermidis* in implant-associated breast tissues of BII subjects. Percentage of Patients with *Cutibacterium acnes* and *Staphylococcus epidermidis* provided above the individual bars. n=8 (normal), n=14 (non-BII), n=46 (BII)
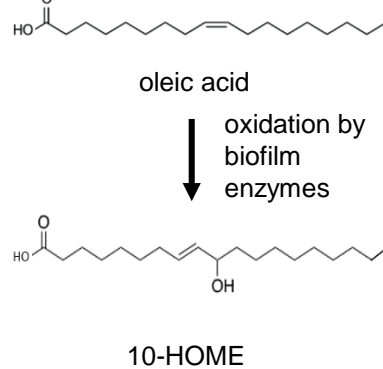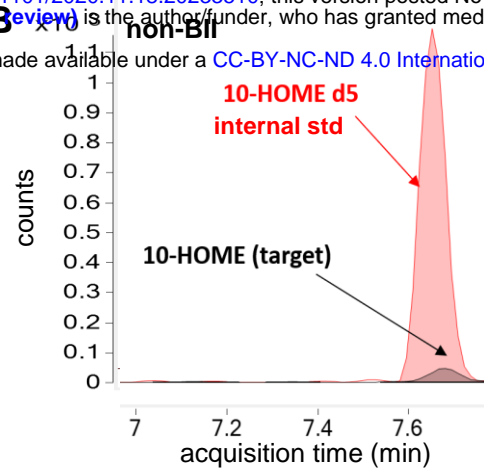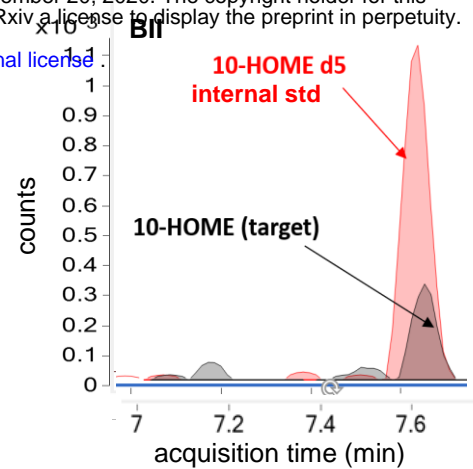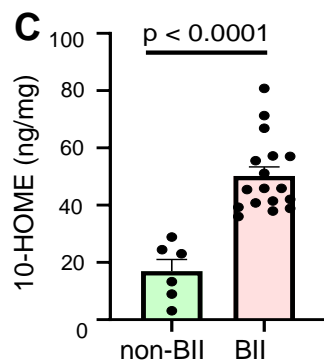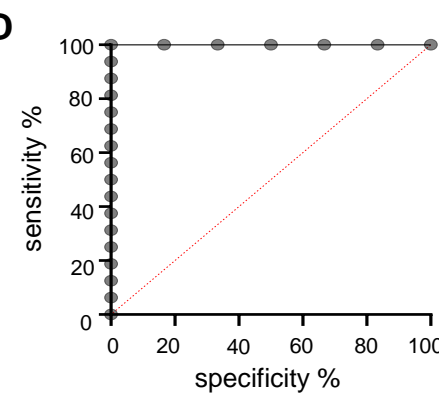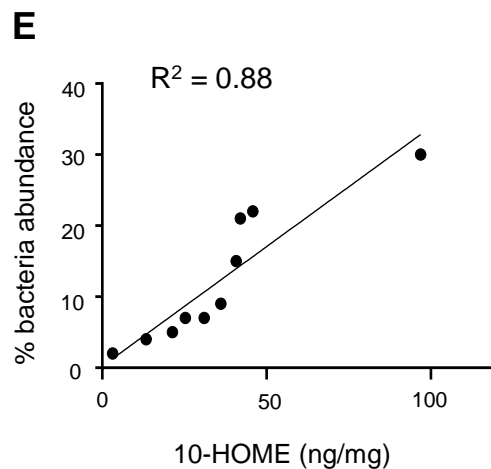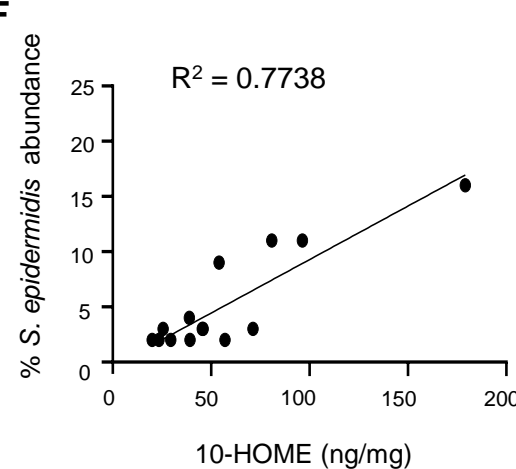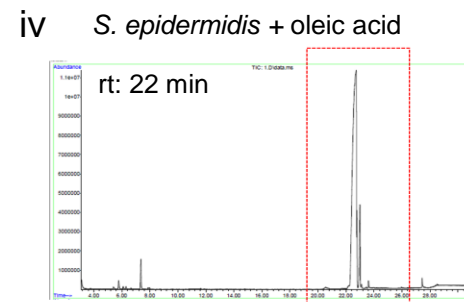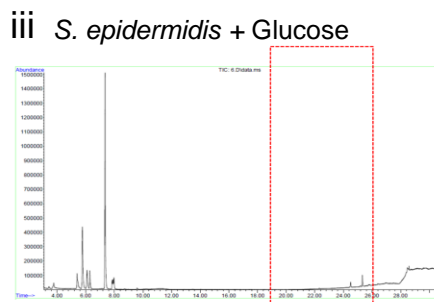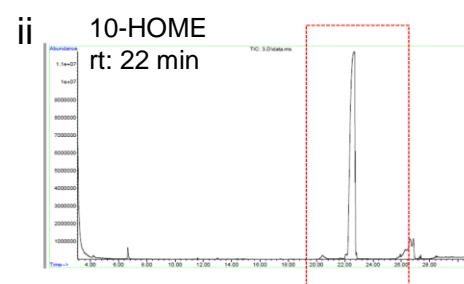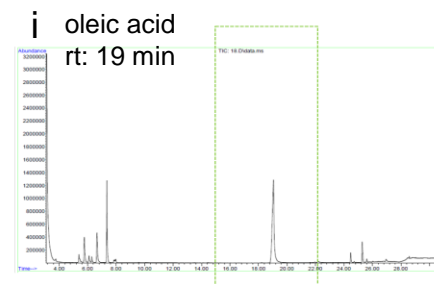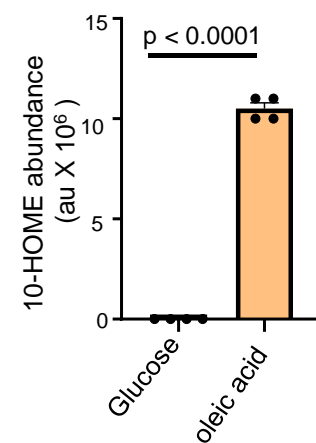
Figure 2

Figure 2 .Increased Abundance of Biofilm Derived 10-HOME in BII Subjects

(A) Schematic of formation of 10-HOME from oleic acid

(B-D) Increased abundance of 10-HOME in implant associated tissue of BII subjects. **B**. Chromatograms of 10-HOME from non-BII and BII using LC-MS/MS targeted analyses. **C**. Data presented as mean ± SEM, n=6 (non-BII), n=17 (BII). **D**. Receiver operating characteristic (ROC) curve analysis to determine specificity and sensitivity of 10-HOME detection.

(E) Increased abundance of bacteria associated with 10-HOME detected from the implant associated tissue of BII subjects.

(F) Increased abundance of *Staphylococcus epidermidis* associated with 10-HOME detected from the implant associated tissue of BII subjects.

(G) Synthesis of 10-HOME by *S. epidermidis in vitro* upon using oleic acid as carbon source. Gas chromatography- mass spectrometry analyses for detection of 10-HOME. **i-** oleic acid standard, **ii-** 10-HOME standard, **iii-** *S.epidermidis* with glucose as carbon source, **iv-** *S.epidermidis* with Oleic acid as carbon source, **v-** quantification of 10-HOME abundance. n=4

Figure 2 .Increased Abundance of Biofilm Derived 10-HOME in BII Subjects
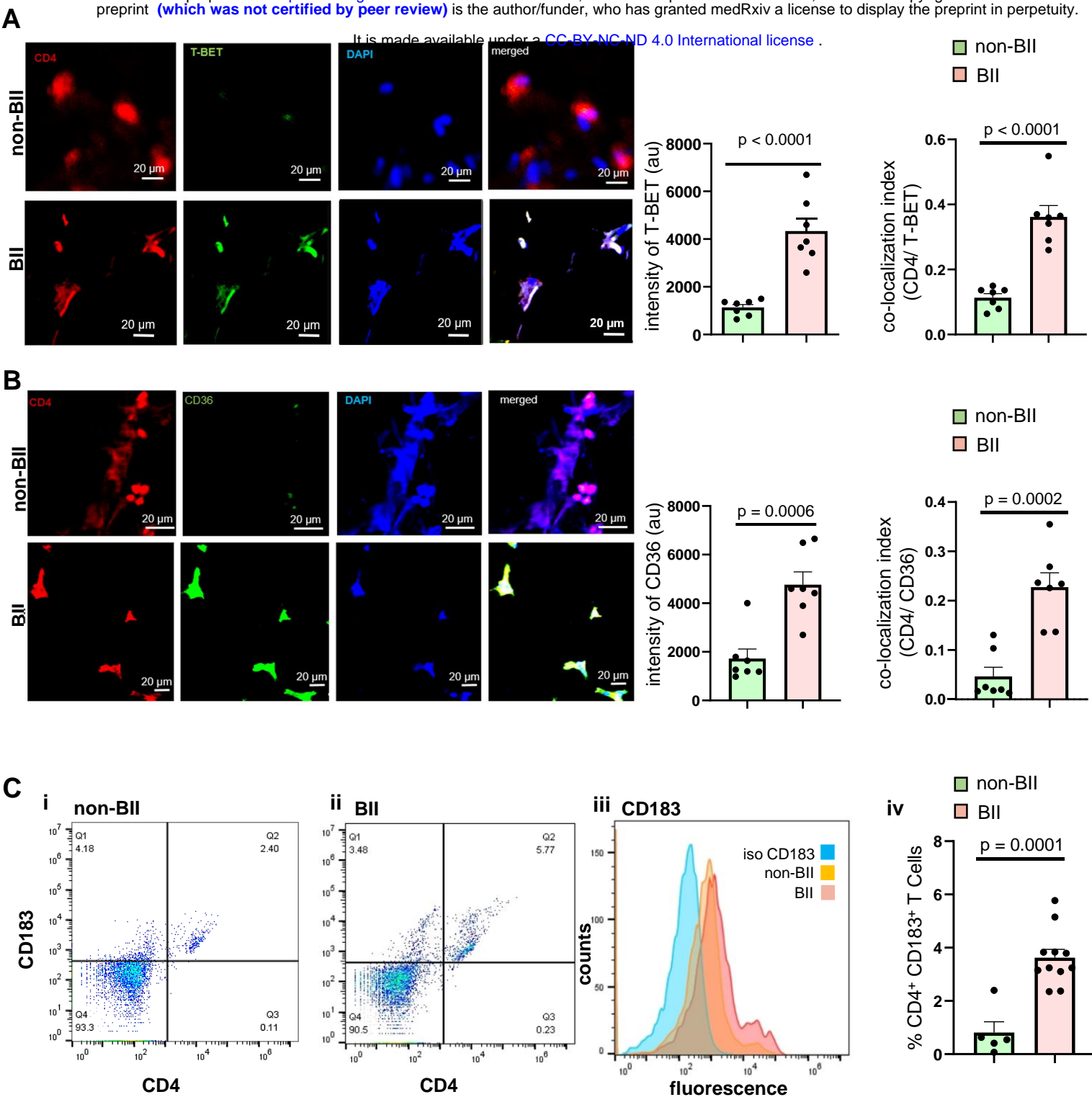
Figure 3

Figure 3. Abundance of CD4+ Th1 Cells in Implant Associated Tissue of BII Subjects

(A) Increased expression of T-BET (transcription factor for Th1 subtype) in breast tissue associated with BII subjects compared to non-BII breast tissue. Breast tissue immuno-stained with anti-CD4 (red) antibody, anti-T-BET (green) and DAPI (blue). Intensity of TBET for the two groups, colocalization of CD4 and T-BET depicted increased abundance of CD4$^+$ TBET$^+$ cells in the breast tissues of BII subjects. Data presented as mean ± SEM, (n=7). Scale bar = 20 µm

(B) Increased expression of CD36 (fatty acyl translocase) in breast tissue associated with BII subjects compared to non-BII breast tissue. Breast tissue immuno-stained with anti-CD4 (red) antibody, anti-CD36 (green) and DAPI (blue). Intensity of CD36 for the two groups, colocalization of CD4 and CD36 depicted increased abundance of CD4$^+$ CD36$^+$ cells in the breast tissues of BII subjects. Data presented as mean ± SEM, (n=7). Scale bar = 20 µm

(C) Elevated Th1 subtype in the peripheral blood of BII subjects. Flow cytometry analyses of peripheral blood of subjects stained with anti-CD4 (FITC) and anti-CD183 (PE). Representative flow plots. (i) non-BII (ii) BII (iii) histogram with isotype control for CD183 (iv) % of CD4$^+$ CD183$^+$ T cells. Data presented as mean ± SEM, (n=5-11).
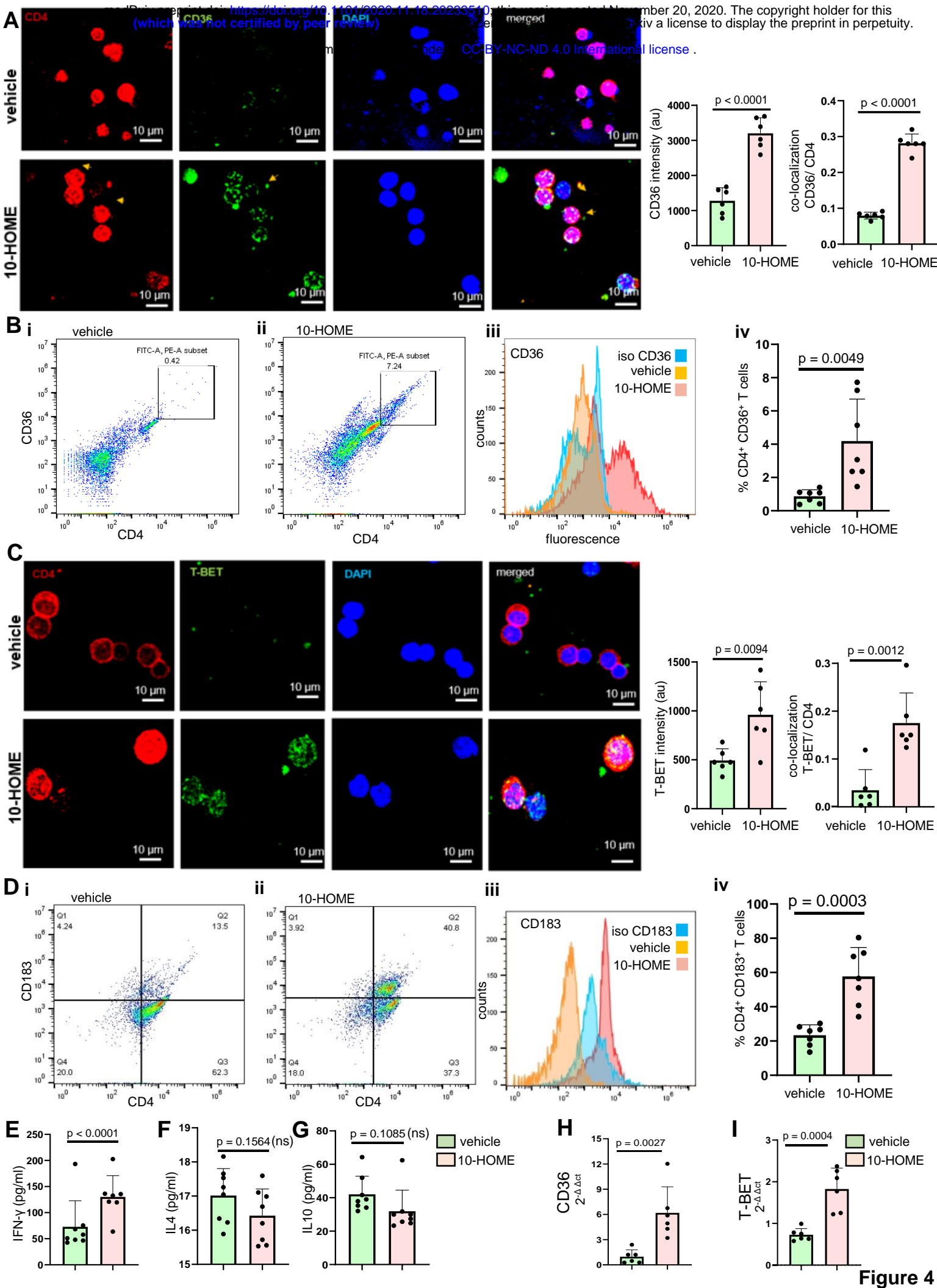
Figure 4

Figure 4. Oxylipin 10-HOME Polarizes Naïve CD4+ T Cells to Th1 Subtype *in vitro*

(A) Increased expression of CD36 in naïve CD4$^+$ T cells treated with 100 µm of 10-HOME compared to vehicle post-48h. T cells were immuno-stained with anti-CD4 (red) antibody, anti- CD36 (green) and DAPI (blue). Intensity of CD36 quantified for the two groups. Colocalization of CD4 and TBET depicted increased abundance of CD4$^+$ CD36$^+$ cells in the breast tissues of BII subjects. Data presented as mean ± SD, (n=6). Scale bar = 10 µm

(B) Elevated CD36 in the 10-HOME treated naïve T cells. Flow cytometry analyses of treated cells stained with anti-CD4 (FITC) and anti-CD36 (APC). Representative flow plots. (i) vehicle treated (ii) 10-HOME treated (iii) histogram with isotype control for CD36 (iv) % of CD4$^+$ CD36$^+$ T cells. Data presented as mean ± SD, (n=7).

(C) Increased expression of T-BET in naïve CD4$^+$ T cells treated with 100 µm of 10-HOME compared to vehicle post-48h. T cells were immuno-stained with anti-CD4 (red) antibody, anti- TBET (green) and DAPI (blue). Intensity of TBET quantified for the two groups. Colocalization of CD4 and TBET depicted increased abundance of CD4$^+$ TBET$^+$ cells in the breast tissues of BII subjects. Data presented as mean ± SD, (n=6). Scale bar = 10 µm

(D) Elevated Th1 subtype (CD183$^+$) in the 10-HOME treated naïve CD4$^+$ T cells. Flow cytometry analyses of treated cells stained with anti-CD4 (FITC) and anti-CD183 (PE). Representative flow plots. (i) vehicle treated (ii) 10-HOME treated (iii) histogram with isotype control for CD183 (iv) % of CD4$^+$ CD183$^+$. Data presented as mean ± SD, (n=7).

(E) Increased expression of Th1 secreted pro-inflammatory cytokine IFN-γ in the 10-HOME treated naïve CD4$^+$ T cells as measured through ELISA. Data presented as mean ± SD (n=7).

(F-G) No significant change in the cytokines IL4 and IL10 following10-HOME treatment of naïve CD4$^+$ T cells as measured through ELISA, Data presented as mean ± SD, (n=8).

(H-I) Increased expression of (H) CD36 (I) T-BET in 10-HOME treated naïve T cells as measured through quantitative real time PCR. Data presented as mean ± SD, (n=6).
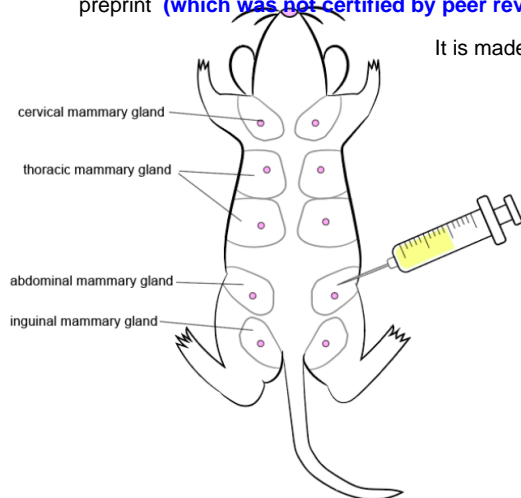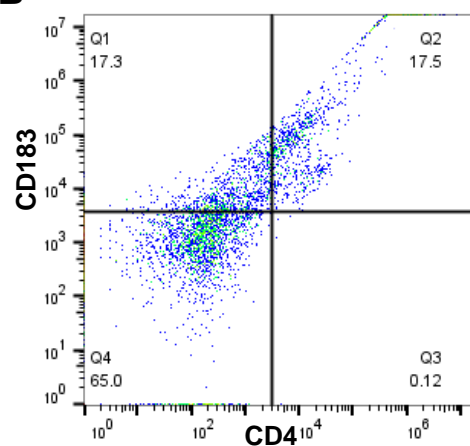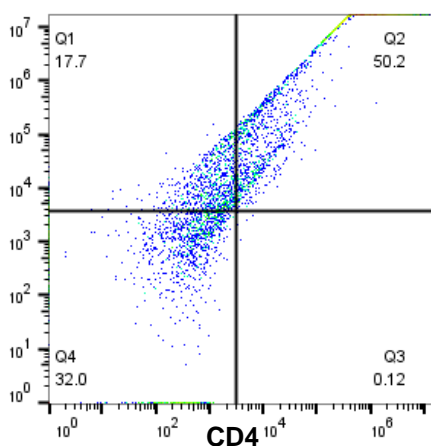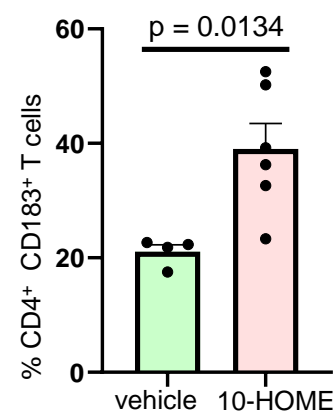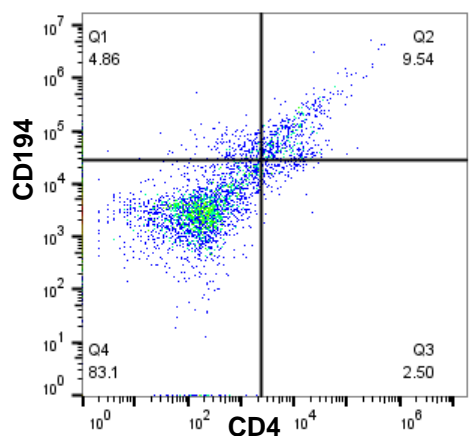
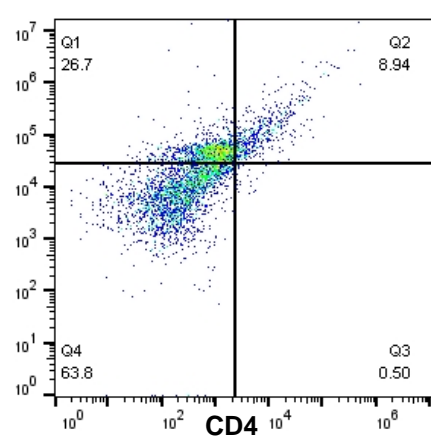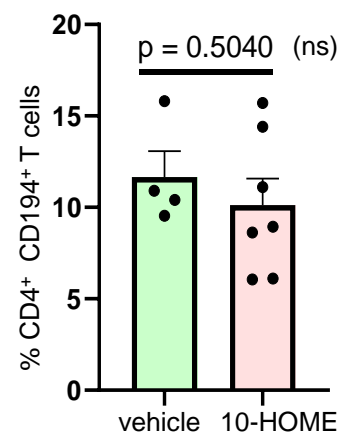**Figure 5**

Figure 5. Elevated CD4$^+$ Th1 in Peripheral Blood of Mice Administered with 10-HOME

(A) Schematic representation of injection of 10-HOME in the abdominal mammary fat pad of mice.

(B) Elevated CD4$^+$ Th1 subtype in the blood of mice injected with 10-HOME. Flow cytometry analyses of blood of mice stained with anti-CD4 (FITC) and anti-CD183 (PE). Representative flow plots. (i) Vehicle treated (ii) 10-HOME treated (iii) % of CD4$^+$ CD183$^+$ T cells. Data presented as mean ± SEM, (n=4-6 mice).

(C) Unaltered CD4$^+$ Th2 subtype in the blood of mice injected with 10-HOME. Flow cytometry analyses of blood of mice stained with anti-CD4 (FITC) and anti-CD194 (PE). Representative flow plots. (i) Vehicle treated (ii) 10-HOME treated (iii) % of CD4$^+$ CD194$^+$ T cells. Data presented as mean ± SEM, (n=4-6 mice).